Original

Zainal, N.; Ramli, H.; Fritz, M.; Abetz, V.; Chan, C.:
Influence of thermal treatment on the properties and intermolecular interactions of epoxidized natural rubber-salt systems.
In: Pure and Applied Chemistry. Vol. 93 (2021) 10, 1119 - 1139.

First published online by De Gruyter: 24.08.2021

https://dx.doi.org/10.1515/pac-2020-0904

Nurul Fatahah Asyqin Zainal, Hairunnisa Ramli, Margarethe Fritz, Volker Abetz, and Chin Han Chan*

Influence of Thermal Treatment on the Properties and Intermolecular Interactions of Epoxidized Natural Rubber-Salt Systems

Abstract: The influence of thermal treatment on the thermal stability, thermal properties, dielectric properties and intermolecular interaction of binary epoxidized natural rubber (ENR)-salt systems, which may be a candidate for solid polymer elec- trolytes (SPEs) was investigated. Solubility of salt in ENR enhances, which may be due to the disruption of the lightly-crosslinked microgel under heat treatment. The increase in the ionic conductivities of the thermally treated ENR SPEs at constant salt content is correlated to the higher glass transition temperatures, development of percolation network and higher extent of intermolecular interactions between ENR and charged entities in this study.

Keywords: thermal treatment; epoxidized natural rubber; macrogel; microgel; glass transition temperature; dielectric properties; intermolecular interaction.

Introduction

Epoxidized natural rubber (ENR) has been utilized for commercial applications (*e.g.* automotive [1], coatings [2, 3], clamping [4] wire and cabling [5], rubber bearing [6], shoe soles [7], binder [8] etc.) due to its inherited features (such as elastomeric and flexibility) and improved properties as compared to natural rubber (NR). Epoxidation on NR, *i.e.* substituting some of the randomly distributed double bonds of along the *cis*-poly(isoprene) backbone with epoxide unit [9–12], enhances the oil resistance, resilience, wet grip and in some cases also for mechanical strength [11–15]. The mol% of epoxide group in ENR is referred as the epoxidation level (*e.g.* ENR-25 marks 25 mol% of epoxide group) [9,16]. ENR is comprised of sol and gel. The sol is the soluble part of polymer chains which is not connected to the network. It is soluble in organic solvents, whereas the gel is a chemically or physically crosslinked network of polymer chains which cannot be dissolved in the solvent in use [11, 17–19]. The presence of a gel domain promotes the elastomeric properties in unvulcanized ENR [18, 20–23].

Existence of nitrogenous compounds (*e.g.* proteins) in NR may play an important role in formation of network-like structure in the gel domain , either *via* hydrogen bonding [18, 20, 24] and/or physical interactions, which occur between phospholipids attached to the α-end of the poly(isoprene) and the proteins at the ω-terminal end of the macromolecules [25, 26]. These network-like structures may be correlated to the gel content of NR [27], where the amount of gel varies from 1 *wt*.% – 25 *wt*.% in different studies [22, 23, 28]. The gel domain comprises two fractions, *i.e*. macrogel and microgel. The macrogel can be separated relatively easy from its sol through simple filtration [29–31]. Macrogel is a term for relatively 'heavy' crosslinked polymer chains of ENRs. Microgel (also known as microaggregates) is lightly crosslinked polymer chains, which presents in ENR with amount less than macrogel. Very often, removal of microgel in NR was neglected or not attempted due to the low content of microgel and also tedious separation procedures involving ultracentrifugation [32, 33], microfiltration [27], mastication [28, 34], etc.

Nurul Fatahah Asyqin Zainal, Hairunnisa Ramli, Centre of Foundation Studies, Universiti Teknologi MARA, Cawangan Selangor, Kampus Dengkil, 43800, Dengkil, Selangor, Malaysia

Margarethe Fritz, Volker Abetz, Department of Physical Chemistry, Universität Hamburg, Grindelallee 117, 20146, Hamburg, Germany

Volker Abetz, Institute of Polymer Research, Helmholtz Zentrum Geesthacht, Max Planck Strasse 1, 21502, Geesthacht, Germany

***Corresponding author: Chin Han Chan,** Faculty of Applied Sciences, Universiti Teknologi MARA, 40450, Shah Alam, Selangor, Malaysia

ENR-salt systems have been studied since the last two decades [35–47] due to the hope for their potential application in rechargeable batteries. This amorphous polymer host has low glass transition temperature (T_g) (*e.g.* T_g of ENR-50 at around −20 °C) [40–42, 46, 47] and existence of epoxide groups which may associate with inorganic salts [38–40], [42, 46, 47]. Previous studies show that ENR-salt systems with higher epoxide content tend to exhibit higher ion conductivity (σ_{DC}) at room temperature due to the presence of more coordination sites for the percolation of charge entities [37, 41]. However, other studies show ENR-25-salt systems exhibit higher conductivities as compared to ENR-50 at salt fraction, W_S = *const* above the solubility limit of ENR-50 ($0.11 < W_S < 0.25$), where $W_S = \frac{\text{mass of salt}}{\text{mass of (ENR + salt)}}$ [40, 42, 43]. This anomalous behavior is suggested to be the result of phase heterogeneity between ENR-50 and lithium perchlorate, $LiClO_4$ mixture due to the maximal solubility, where the salt-poor phase (*i.e.* the microgel domain) does not show dielectric response [46]. Therefore, the maximum order of the ionic conductivity of ENR-50-salt systems ($\sigma_{DC} \sim 10^{-8}$ S cm^{-1}) is observed to stay constant within $0.11 < W_S < 0.25$, meanwhile ENR-25-salt systems show an increase in conductivity up to $W_S < 0.17$ ($\sigma_{DC} \sim 10^{-7}$ S cm^{-1}).

Separation of gel from ENR sol is a crucial step in preparation of ENR-salt samples. This is because the gel domain may limit the salt penetration into the polymer coils, which is important for intermolecular interaction between epoxide groups in ENR and the charged entities [48]. In some studies, simple filtration was adopted in order to remove macrogel from ENR sol [32, 40–43, 46, 49, 50]. As for the removal of the microgel domain , ultracentrifugation followed by filtration through 0.45–μm pore size and ultrafiltration through 0.20–μm were applied in some cases [27, 51]. However, the latter procedure is not viable for commercial application.

The ionic conductivity of high molar mass ENR-salt systems is known to be governed by the differences in epoxide content of ENR [37, 41, 42], gel content of ENR [52], effect of non-rubber components (*e.g.* protein and phospholipids) [52], sample preparatory pathway [43], etc. We focus on the effect of regulating the microgel content by thermal treatment on dielectric properties of ENR-salt systems. $LiClO_4$ salt was used in this study due to its less hygroscopic nature and stable in ambient moisture as compared to other Li salts (*e.g.*, Li SO_3CF_3, $LiPF_6$, $LiBF_4$, *etc.*) [53–56], low lattice energy [53, 54], and acceptable electrochemical stability [53, 57]. Studies on Li salts with different anions (*e.g.*, Cl^-, ClO_4^-, $TFSI^-$, PF_6^-, *etc.*) [55, 58, 59] describe the large polyatomic anions (*e.g.*, ClO_4^- and $TFSI^-$) with delocalized electron charge has a weak interaction with Li^+, which facilitates the dissociation between the cations and anions, and consequently promoting high solubility in polymer. Li^+ with larger anion such as $TFSI^-$, shows higher interaction with polymer [55,58–60], however, it has high hygroscopicity property, which is quite challenging for us to control the moisture absorption under our experimental conditions. In our previous study [43], ENR-salt systems were thermally treated for the enhancement of ionic conductivity of the systems without removal of microgel. The 'lightly crosslinked' microgel domain in ENR may be disrupted by thermal treatment at 80 °C for sufficiently long duration. This may lead to better solubility of salt at low salt concentrations in ENRs, especially for ENR-50 at W_S = *const*. Influence of thermal treatment on gel content, molar masses and thermal stability for neat ENRs will be elucidated. Thermal properties, dielectric properties and intermolecular interactions of the thermally treated binary ENR-salt systems will be scrutinized subsequently.

Experimental Section

Materials

Table 1 summarizes the properties of the materials used. $LiClO_4$ was dried at 100 °C for 24 h prior usage. ENR-25 and ENR-50 were purified before further use by dissolution in tetrahydrofuran (THF) (Merck, Darmstadt, Germany). Macrogel was removed by filtrating ENR sol through ~10-μm nylon filter. Then, the filtered ENR sol was precipitated in methanol (Merck, Darmstadt, Germany). The sample was dried at 50 °C for 24 h before further dried under vacuum at 25 °C for 24 h. This ENR was termed as filtered ENR with removal of macrogel (*i.e.* still consists of microgel), or we simply refer it to ENR.

Table 1: Properties of materials used.

Material	ENR-25	ENR-50	$LiClO_4$
T_g [a] (C)	–43	–23	-
Molecular structure	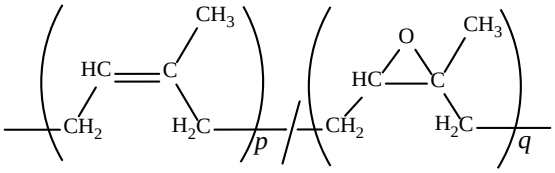 For ENR-25: p = 0.75, q = 0.25 For ENR-50: p = 0.5, q = 0.5		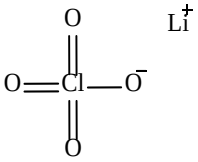
Supplier	Malaysian Rubber Board (Sungai Buloh, Selangor, Malaysia)		Sigma-Aldrich Chemical Co. (St. Louis, MO, USA)

[a] Glass transition temperature during the first heating run.

Preparation of Samples

ENR consisting of different $LiClO_4$ concentrations, $W_S = \frac{\text{mass of salt}}{\text{mass of (ENR + salt)}}$ was dissolved in THF (Merck, Darmstadt, Germany) and stirred for 48 h at 50 °C or until a homogenous solution was obtained. The solution was poured in Teflon® dish and left at room temperature until solvent evaporated. Then, the sample was dried at 50 °C for 24 h. This was followed by isothermal treatment under nitrogen atmosphere at 80 °C with different annealing times, t = 0 and 24 h (*i.e.* without and with thermal treatment) before further drying in vacuum at 25 °C for 24 h. The sample was kept in dessiccators at 25° C. The sample was vacuum dried again at 25 °C for 24 h before sample characterization.

Estimation of Gel Content

4% (*m/m*) of ENR was dissolved in THF and stirred for 48 h at 50 °C or until a homogenous solution was obtained. The solution was filtered using 10–μm nylon filter for removal of macrogel. The first insoluble portion (*i.e.* macrogel) was dried at 50 °C to constant mass. The filtrate on the other hand was concentrated using rotary evaporator and then was precipitated in methanol and dried at 50 °C for 24 h, followed by drying at 50 °C for 24 h and finally was vacuum dried at 25°C for 24 h.

1% (*m/m*) of the dry filtered (macrogel-free) ENR was dissolved in THF for 48 h. The microgel fraction was separated by centrifugation (Kubota 5500, Tokyo, Japan) at 10,000 rpm for 30 min. The solution was then filtered through a 0.45–μm Teflon® membrane filter (Merck Millipore, Burlington, MA, USA). The second insoluble portion (*i.e.* microgel) was dried at 50 °C to constant mass. The purified ENR solution was concentrated using rotary evaporator and then was dried at 50 °C for 24 h and finally was vacuum dried at 25 °C for 24 h. This ENR was termed as purified ENR with removal of macrogel and microgel. We note here that the (purified) ENR was used to prepare all the ENR-salt systems and for all further analyses.

The estimation of macrogel and microgel content was made in at least three replicates as shown in Eq. (1) and Eq. (2).

$$\text{Macrogel content} = \frac{\text{mass of dried macrogel}}{\text{mass of ENR}} \times 100\ \% \quad (1)$$

$$\text{Microgel content} = \frac{\text{mass of dried microgel}}{\text{mass of ENR}} \times 100\ \% \quad (2)$$

Visual Inspection on Solubility of ENR after Thermal Treatment

Visual inspection on the solubility of (macrogel-free) 0.5 g of ENR in 50 mL THF at 25°C after isothermal treatment under N_2 gas at 80 °C at different annealing times was made at 30-min time interval using Canon Camera EOS 400D (EOS Digital X) (Ōta, Tokyo, Japan) equipped with a Tamron 90 mm f/2.8 Di Macro Lens (Saitama, Kantō, Japan).

Gel Permeation Chromatography (GPC)

2% (*m/v*) of neat ENR was dissolved in high performance liquid chromatography (HPLC) grade THF (VWR International, Radnor, Pennsylvania, USA) at 25 °C overnight or until the polymer was completely dissolved. The sample was filtered with 0.2–μm Teflon® membrane filter (Sartorius AG, Göttingen, Germany) for removal of microgel before injecting the sample into GPC. The mass-average molar mass ($\overline{M_w}$) and number-average molar mass ($\overline{M_n}$) were estimated by GPC at 30 °C using Agilent 1260 GPC/SEC (Polymer Standard Service GmbH, Mainz, Germany) coupled with 10^3 Å, 10^5 Å and 10^6 Å of styrene-divinylbenzene gel columns (Polymer Standard Service GmbH, Mainz, Germany), differential refractometer detector RID model G1362 A (Polymer Standard Service GmbH, Mainz, Germany) and UV-Vis detector with wavelength, λ = 260 nm (Polymer Standard Service GmbH, Mainz, Germany). HPLC–grade THF was used as eluent at a flow rate of 1 mL min^{-1}. Polystyrene standards ($\overline{M_w}$= 682 – 2,570,000 g mol^{-1}) with dispersity ($Đ$) = 1.05 were used for calibration (Polymer Standard Service GmbH, Mainz, Germany).

Proton Nuclear Magnetic Resonance (^{1}H-NMR) Spectroscopy

1% (*m/v*) of filtered ENR in deuterated chloroform ($CDCl_3$) (Merck, Darmstadt, Germany) was heated overnight at 50 °C or until the polymer completely dissolved. The sample was filtered with 0.45-μm Teflon® membrane filter (Merck Millipore, Burlington, MA, USA) for removal of microgel. ^{1}H-NMR measurement was performed at 25 °C using Bruker Avance 500 Ultrashield NMR Spectrometer (Billerica, MA, USA) with resonancy frequency of 500 MHz. The chemical shift (δ) of the sample was referenced to δ = 7.26 ppm for $CHCl_3$. Epoxide content of ENR was estimated using Eq. (3),

$$\text{Mol (\%) epoxide} = \frac{A_{2.70}}{A_{5.14}+A_{2.70}} \tag{3}$$

where $A_{2\,70}$ and $A_{5\,14}$ are the intergrated areas of methyne proton of epoxide group and unsaturated methyne proton, respectively.

Fourier-Transform Infrared (FTIR) Spectroscopy

FTIR spectra of the samples were recorded using attenuated total reflection accessory (ATR) on Nicolet iS10 ATR-FTIR Spectrometer (Thermo Fisher Scientific, Waltham, MA, USA) equipped with a diamond crystal over the range of 600 – 4000 cm^{-1} by averaging 16 scans at a maximum resolution of 2 cm^{-1} at 25 °C.

The epoxidation content of filtered ENR was estimated using Eq. 4,

$$\text{mol (\%) epoxidation} = \frac{100k_1A_2}{A_1+k_1A_2+k_2A_3} \tag{4}$$

where $A_1 = A_{837}$, $A_2 = A_{879} + 0.14{\cdot}A_{837}$ and $A_3 = A_{3460} + 0.019{\cdot}A_{1377}$ were deduced from Lambert-Beer law. A_{837}, A_{879}, A_{1377}, and A_{3460} are the absorbances in FTIR spectra at 837 cm^{-1}, 879 cm^{-1}, 1377 cm^{-1} and 3460 cm^{-1}, which correspond to CH olefin out-plane deformation, oxirane ring, CH_3 deformation and hydroxyl group, ν(OH), respectively. The values of k_1 and k_2 are constants determined using NMR method adopted from ref. [19] with values of 0.77 and 0.34, respectively.

Thermogravimetric Analysis (TGA)

TGA Q500 (TA Instrument, Pittsburgh, PA, USA) was used to study the thermal stability [*i.e.* decomposition temperature (T_d) and activation energy of thermal degradation (E_A)] of filtered ENR. The sample was heated from 30 to 600 °C at 10 °C min^{-1} under nitrogen atmosphere. The decomposition temperature of polymer at the onset ($T_{d,onset}$), inflection ($T_{d,inflection}$) and total mass loss were extracted from the thermogram of TGA. $T_{d,onset}$ is defined as the onset of mass loss curve as a function of temperature and $T_{d,inflection}$ is defined as the temperature of maximum composition rate of the mass loss curve for TGA.

Differential Scanning Calorimetry (DSC)

TA Q2000 (TA Instruments, New Castle, DE, USA) equipped with RCS90 refrigerator cooling system (TA Instruments, New Castle, DE, USA) and nitrogen gas purging was used to determine the values of glass transition temperature (T_g) and change in heat capacity (ΔC_p) of the systems in the heating cycle. The DSC was calibrated with indium and sapphire standards. The sample was quenched to –90 °C and kept for 5 min and heated to 80 °C at a rate of 10 °C min^{-1}. A similar thermal procedure was applied for the sapphire standard and baseline runs.

The glass transition temperature T_g was determined using Moynihan's approach [53–56] due to the presence of

relaxation endotherm which is overlaid to the glass transition. To determine the heat capacity C_p value of a sample, the heat flow signal from the sample was compared to the baseline correction experiment whereby an empty reference and an empty sample pan were placed in the furnace. The change of heat capacity ΔC_p was determined from the onset and endset of the glass transition heat flow curve.

Impedance Spectroscopy (IS)

Impedance measurements at 25 °C were determined by using HIOKI 3532-50 Hi-Tester (Nagano, Chūbu, Japan) interfaced with a computer for data acquisition over the frequency range between 50 Hz and 2 MHz. The thin film was sandwiched between two stainless steel disk electrodes (2–cm diameter), which acted as blocking electrodes for ions. The conductivity σ_{DC} was calculated by adopting equation, $\sigma_{DC}=\frac{L}{R_b A}$, where L is the thickness of the ENR film, R_b is the bulk resistance of the electrolyte and A is the area of electrodes. The σ_{DC} value was either estimated from Nyquist plots or from the values of real (Z') and imaginary parts (Z'') of impedance at the frequency for a fully stabilized network ($f^{Z''}_{max}$) [$Z'(f^{Z''}_{max})$ and $Z''(f^{Z''}_{max})$] at maximum of Z''. The values of σ_{DC} were the average calculations of four impedance analyses from different spots of the sample with an error of about 10%.

Results and Discussion

^{1}H-NMR and FTIR Spectroscopies

^{1}H-NMR and FTIR spectra of ENRs are presented in Fig. 1 and Fig. 2. ^{1}H-NMR spectra in Fig. 1 depicts the *cis*-units by the characteristic signals of methyl, methylene and unsaturated methyne protons at 1.71, 2.06 and 5.14 ppm, respectively. Presence of epoxide content in ENR provides a new characteristic signal of methyl and methylene at 1.30 ppm and 2.69 ppm. A broadening of the strong signal at 2.69 ppm in ENR-50 spectrum can be seen in Fig. 1(b). This may be due to higher amount of oxygen of epoxide group in ENR-50 as compared to ENR-25 which exhibits a strong signal at 5.14 ppm.

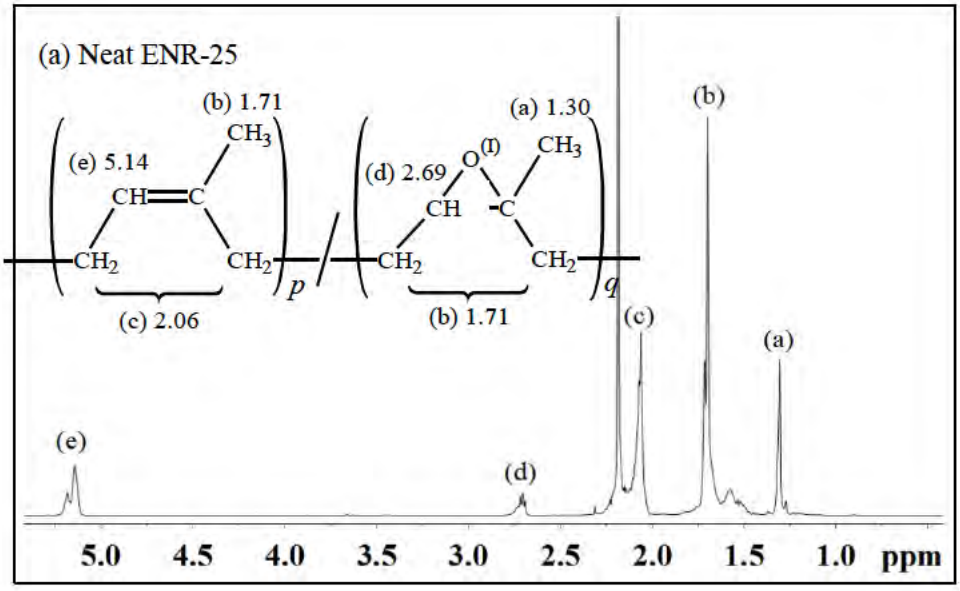

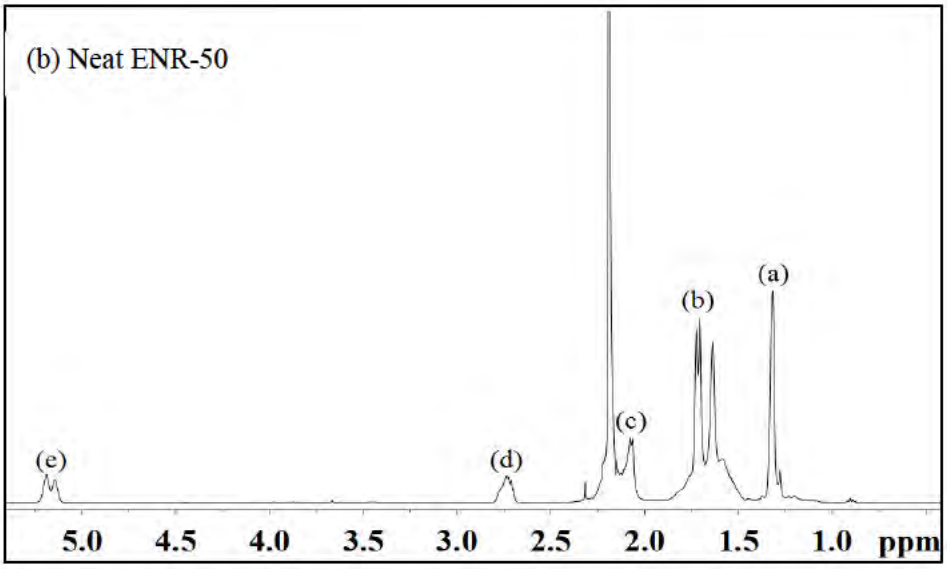

Fig. 1: ^{1}H-NMR spectra of (a) ENR-25 and (b) ENR-50.

In Fig. 2, absorption bands of *cis*-1,4-polyisoprene of ENR, which appear at 837 cm^{-1}, 1377 cm^{-1} and 1664 cm^{-1} reflect the CH olefin out-plane deformation (ωHC=), CH_3 deformation (νCH_3) and C=C stretching (νC=C), respectively [10, 19, 57]. Meanwhile, the presence of the absorption bands at 879 cm^{-1} (oxirane ring) [19] and 1069 cm^{-1} (vibration of C–O–C stretching, νC–O–C) can be attributed to the epoxide group of ENR. The spectrum of ENR-25 [Fig. 2(a)] shows strong absorption band at 837 cm^{-1} as compared to 879 cm^{-1}. This illustrates that the mol% of unsaturated sites in ENR-25 is higher as compared to epoxide sites, which appears adversely in the spectrum of ENR-50 [Fig. 2(b)].

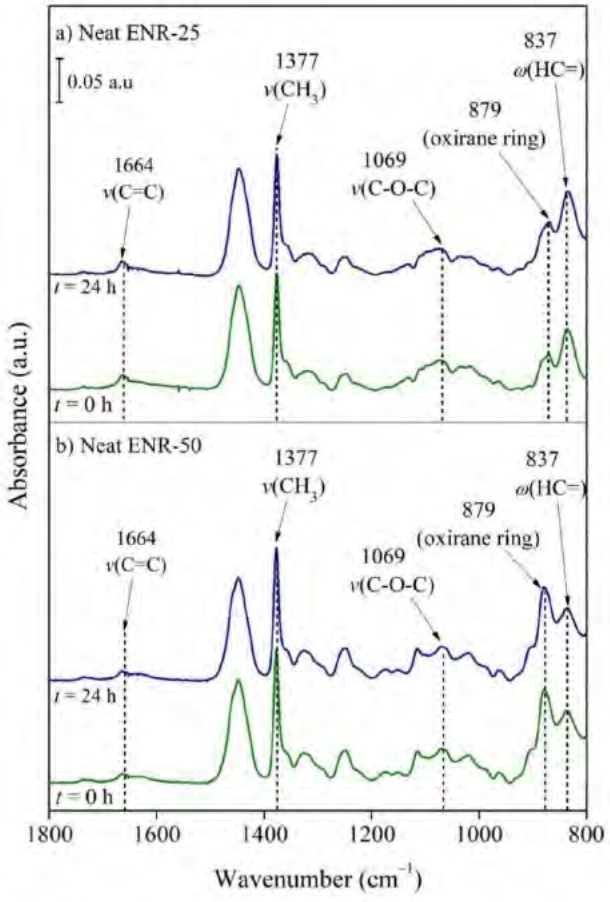

Fig. 2: FTIR spectra of (a) ENR-25 and (b) ENR-50, at $t = 0$ and 24 h.

Both ^{1}H-NMR and FTIR spectra of ENR-25 and ENR-50 may reveal the molecular structure of ENRs. The epoxide content of ENR determined by ^{1}H-NMR agrees well with the reported epoxide content of the commercial ENR (Table 2). Nevertheless, ATR-FTIR remains a convenient tool to differentiate commercial ENR-25 and ENR-50 rapidly without any special sample preparation. Isothermal treatment of ENR-25 and ENR-50 at 80 °C for 24 h does not have a significant effect on the epoxide content of the ENR, which is illustrated in Fig. 2(a), Fig. 2(b) and Table 2.

Table 2: Epoxide content for ENRs.

ENR	Estimated epoxide content (mol%)		
	^{1}H-NMR	FTIR	
		t = 0 h	t = 24 h
ENR-25	25 ± 1	29.2 ± 0.5	28.7 ± 0.6
ENR-50	50 ± 3	44.5 ± 0.1	44.6 ± 0.2

Estimation of Gel Content

The existence of non-isoprene compounds in NR [66] or ENR and the higher polarity of the epoxide group in ENR are assumed to be involved in the interaction between the polymer chains, leading to the existence of a gel content [9, 15]. Table 3 demonstrates the macrogel and microgel content of ENR.

Table 3: Gel content of ENRs.

Gel content (% *m*/*m*)	ENR-25	ENR-50	ENR-60
Macrogel	7.2 ± 0.4	9.9 ± 1.0	55.0 [a] 89.0 [b]
Microgel	1.8 ± 0.7	2.8 ± 1.3	-

[a] Data taken from [67].
[b] Data taken from [32]. Standard deviations were not reported.

Both macrogel and microgel content of ENR-50 is higher than ENR-25. Similar observations were also reported in [21, 59–61], where higher epoxidation levels of ENR yield higher gel contents. During the epoxidation reactions, further ring-opening reaction of epoxide groups is also possible [19]. Typically, acidity, high temperature and the level of ENR epoxidation are the main factors for the formation of the ring-opening reaction [10, 19]. The ring-opening of epoxide may form ether crosslinks (*i.e* intermolecular ether), which lead to the formation of gel [9, 32]. The formation of the intermolecular ether increases with higher epoxidation level of ENR [19]. Furthermore, the increase in gel content may also be attributed to the ring-opening of epoxide groups and reaction with non-isoprene compounds (*i.e* proteins and phospholipids) to form three-dimensional network structures [9, 62, 63]. Consequently, the formation of these network structures increases the T_g of ENR due to suppression of polymer chain mobility [72]. This is in agreement with the results of this study, where the T_g of ENR-50 is higher than ENR-25 (*c.f* section Glass Transition Temperature) due to higher gel content in ENR-50.

Very high gel content (> 50 wt.%) of ENR-60 reported in ref. [67] which may involve complex and tedious purification procedures to remove the gel. This is not viable to be used in commercial applications. Hence, the highest epoxide content of commercial ENR is 50 mol %.

Visual Inspection on Solubility of ENR after Thermal Treatment

The thermal treatment of ENR at 80 °C under inert atmosphere may disrupt the 'lightly crosslinked' polymer chains (*e.g*. microgel). The disruption of microgel in ENR after extended thermal treatment time may speed up the solubility of ENR in solvent.

Selected micrographs of dissolution of ENR in THF at 25 °C are displayed in Table 4. The visual inspection of the micrographs suggests that the dissolution of ENR-50 in THF is slower as compared to ENR-25 due to higher microgel content in ENR-50 with and without thermal treatment. After thermal treatment, the complete dissolution of

ENR-25 occurs roughly at a dissolution time in THF (t_{THF}) of 90 min, whereas ENR-50 at 150 min. Thermally treated ENRs dissolve faster in THF due to the disruption of 'lightly crosslinked' polymer chains. This may suggest that ENRs with disrupted microgel which dissolve faster, may lead to more dissolved lithium salt in thermally treated ENRs as suggested in ref. [43]. The samples' film and schematic diagrams of both ENRs with and without thermal treatment are shown in Figure 3 which illustrates the effect of thermal treatment on the disruption of 'lightly crosslinked' ENR chains. As shown, the films do not display any color change upon thermal treatment.

Table 4 Visual inspection of dissolution of ENR in THF at 25 C as a function of t_{THF}. White arrows indicate complete dissolution of ENR in THF.

(t_{THF})	ENR-25		ENR-50	
	t = 0 h	t = 24 h	t = 0 h	t = 24 h
0 min				
90 min				
150 min				
270 min				

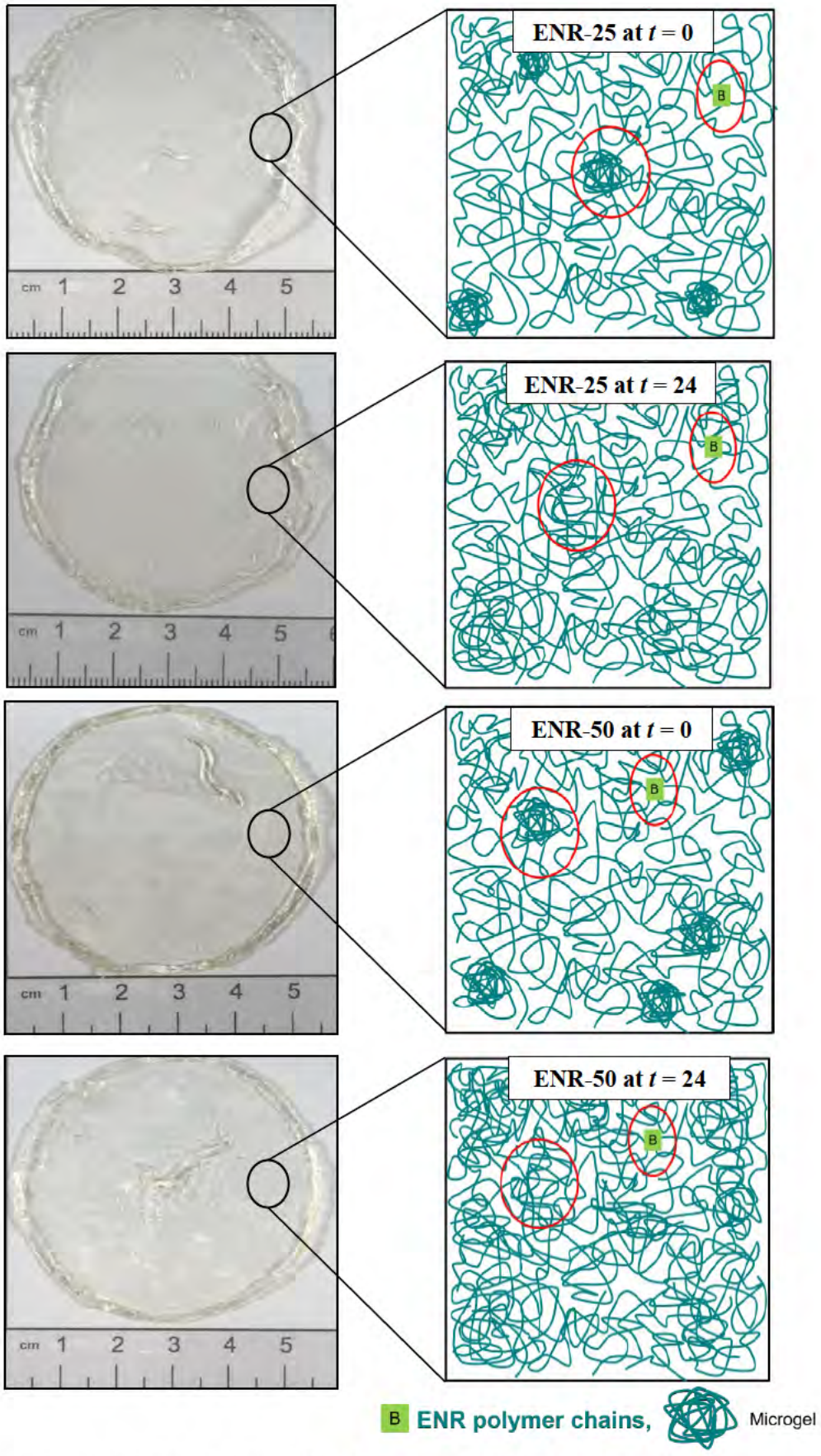

Fig. 3: Samples' films and schematic diagrams of both ENRs annealled at $t = 0$ h and $t = 24$ h

Molar Masses of ENRs

Quantities of apparent weight averaged molecular weight $\overline{M_w}$ for ENR-25 and ENR-50, with or without thermal treatment are roughly 400 kg mol^{-1} with dispersity ($\overline{M_w}/\overline{M_n}$) around 3 – 4. Isothermal treatment at 80 °C for 24 h under inert condition has no significant effect on the average chain length of the ENRs.

Thermal Stability of ENRs

Fig. 4 and Fig. 5 show the thermograms of ENR-50 annealed at $t = 0$ and 24 h and semi-logarithmic plots of ln(|deriv. mass retained (%)|) *versus* $1/T$ for ENR-25 and ENR-50, respectively. Results are tabulated in Table 5.

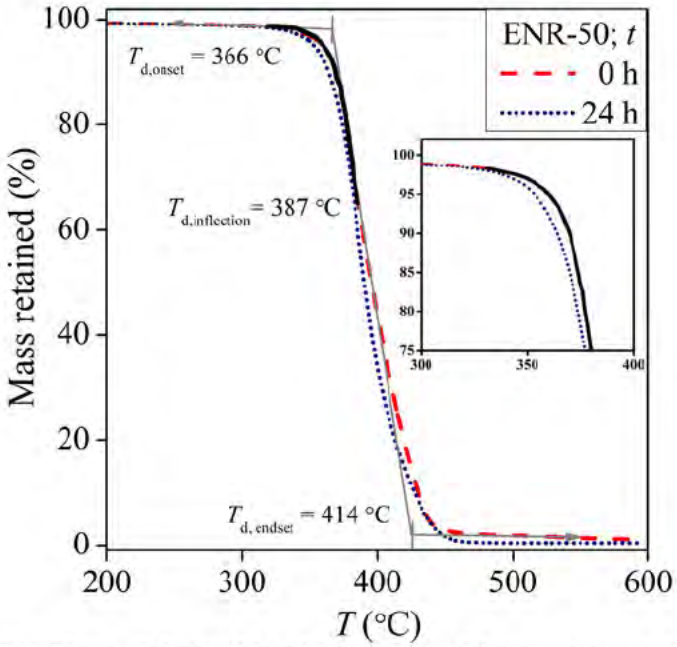

Fig. 4: Thermograms of ENR-50 annealed at $t = 0$ h and 24 h. Black solid curve represents the selected region used for estimation of E_A after Eq. 5. Inset figure shows the selected region for estimation of E_A.

Single-stage mass loss is observed in the thermograms of ENR-50 as shown in Fig. 4. A drastic decrease in mass retained of ENR-50 is observed at $T > 300$ °C indicates that ENR is thermally stable up to roughly 300 °C. Similar observation is noted for ENR-25. Insignificant changes are seen for $T_{d,onset}$ and $T_{d,inflection}$ between ENR-25 and ENR-50 in Table 5 with or without thermal treatment.

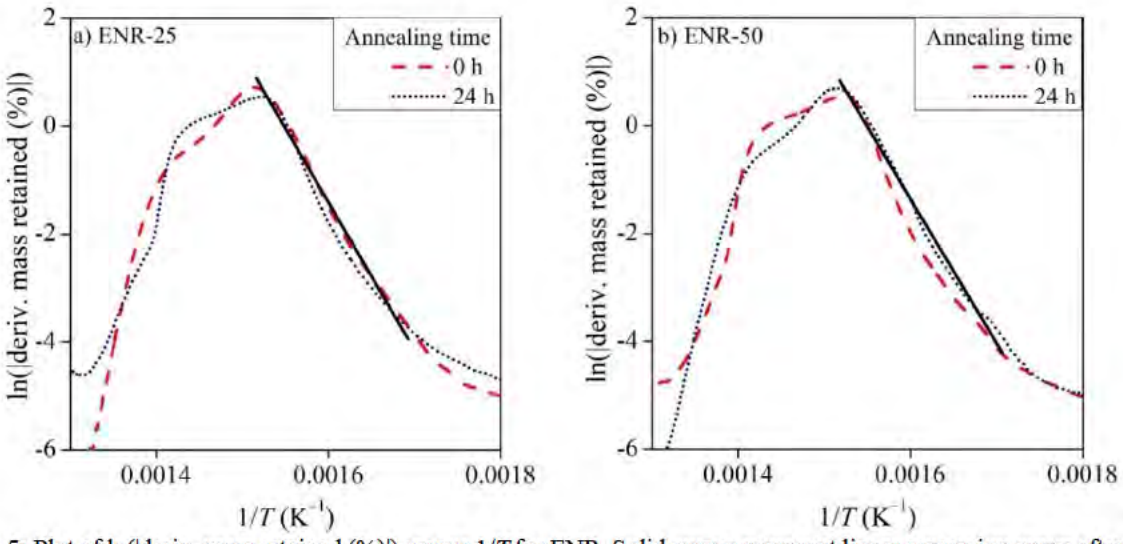

Fig. 5: Plot of ln(|deriv. mass retained (%)|) *versus* $1/T$ for ENR. Solid curves represent linear regression curve after Eq. (5).

Temperature-dependence of the rates of thermal degradation for ENR-25 and ENR-50 were evaluated using the Hoffman's Arrhenius-like relationship shown in Eq. (5). Estimation of E_A from initial stage of the decomposition (*i.e.* solid curves in Fig. 4 and Fig. 5) is tabulated in Table 5. The confidence intervals of the E_A refer solely to the regression analysis using two-tailed student *t*-test with 95 % of confidence level for one experiment.

$$|\text{deriv. mass retained (\%)}| \; \alpha \; \exp\left(-\frac{E_A}{RT}\right) \tag{5}$$

Table 5: $T_{d,onset}$, $T_{d,inflection}$ and E_A of ENRs.

t	ENR-25			ENR-50		
	$T_{d,onset}$ (C)	$T_{d,inflection}$ (C)	E_A (kJ mol^{-1})	$T_{d,onset}$ (C)	$T_{d,inflection}$ (C)	E_A (kJ mol^{-1})
0 h	368	387	271 ± 0.5	370	385	320 ± 0.1
24 h	366	387	263 ± 1.0	368	385	265 ± 0.4

The E_A value of thermal degradation of ENR-50 is slightly higher than ENR-25. In other words, ENR-50 is thermally more stable than ENR-25. Quantity E_A of ENR without thermal treatment is slightly higher than ENR with thermal treatment. ENRs with thermal treatment is thermally less stable as compared to ENRs without thermal treatment, which may be due to the disrupted 'lightly crosslinked' polymer chains with lower thermal stability. Higher thermal stability is associated to the higher crosslink density of polymer chains. This is observed in ref. [65–67] where vulcanized NR shows higher thermal stability as compared to unvulcanized NR.

Glass Transition Temperatures

Thermal treatment of neat ENR-25 and ENR-50 at 80 °C does not change the T_g values of ENRs significantly (*c.f.* Fig. 6). When $LiClO_4$ is added, segmental motion of ENR chains is restricted due to the intermolecular interaction between ENR and salt (*c.f.* Intermolecular Interactions). Besides, ENR-50 has a higher increase in T_g values at W_S = *const* as compared to ENR-25. The extent of solubility of salt in the polymer may be correlated to the amount of epoxide units in ENR.

On top of that, upon thermal treatment, at W_S > 0.065, higher solubility of salt in ENRs and thus increase in T_g can be observed. This effect is especially pronounced for ENR-50. This may be due to higher amount of microgel in ENR-50 is "disrupted" (*c.f.* Table 2) after thermal treatment, which may lead to more salt dissolving in ENR-50.

Investigation on the Li ions mobility and interaction with polymer using ^{7}Li NMR spectroscopy was widely studied [60,76–80]. Nevertheless, the analogue qualitative analysis based on T_g from DSC data to elucidate the interaction between Li ions and polymer is equivalently useful. Experiments show an increase in T_g with ascending salt content and constancy in ΔC_P with it. The change in T_g is discussed in thermodynamic terms [64], where the discussion adopts elements of the Gibbs and DiMarzio approach [81]. In general, an increase in T_g implies reduction of segmental mobility of polymer chains [69, 70]. T_g increases up to the saturation of the polymer-salt mixture [71, 72]. Above saturation of the polymer-salt mixture, the system separates into polymer-rich and salt-rich phases.

Below the saturation of the polymer-salt mixture, addition of salt to polymer may lead to change the glass transition temperature from T_g^o to T_g. For ΔC_P = *const*,

$$\ln\left(\frac{T_g}{T_g^o}\right) = -\frac{\Delta S^{glass}}{\Delta C_P} \tag{6}$$

where T_g^o is the glass transition temperature of neat polymer and ΔS^{glass} is the change in entropy of the glassy state after addition of salt which describes the further deviation from equilibrium.

When the reduced glass transition temperature (the left-hand side) is greater than unity, $\Delta S^{glass} < 0$ because ΔC_P > 0 is observed. In other words, when T_g/T_g^o > 1 (addition of salt to polymer leads to increase of T_g of polymer-salt mixture), entropy $-\Delta S^{glass}$ reflects freezing in of chain's degree of freedom by addition of salt. Reduced T_g may also be expressed by

$$\frac{T_g}{T_g^o} = 1 + \frac{\Delta T}{T_g^o} \qquad \text{where } \Delta T \equiv T_g - T_g^o \tag{7}$$

and for small $\Delta T/T_g^o$ Eq. (6) can be rewritten as

$$-\Delta S^{\text{glass}} = \Delta C_{\text{P}} \frac{\Delta T}{T_{\text{g}}^{\text{o}}} \tag{8}$$

Linear dependency of T_{g} with respect to W_{S} can be expressed by

$$\frac{T_{\text{g}}}{T_{\text{g}}^{\text{o}}} = 1 + \frac{1}{T_{\text{g}}^{\text{o}}}\left(\frac{\partial T_{\text{g}}}{\partial W_{\text{S}}}\right) W_{\text{S}} \qquad \text{with } W_{\text{S}} \ll 1 \tag{9}$$

where the slope, Γ is $\frac{1}{T_{\text{g}}^{\text{o}}}\left(\frac{\partial T_{\text{g}}}{\partial W_{\text{S}}}\right)$. Parameter Γ for both ENR-salt systems obtained from the linear regression after Eq. (9) are presented in Fig. 6. The relationship of Eq. (6) and Eq. (9) suggests that the parameter Γ is closely connected to partial molar entropy of the polymer in the polymer-salt mixture, $\Delta\tilde{S} \equiv \frac{\partial \Delta S^{\text{glass}}}{\partial W_{\text{S}}}$. It follows

$$-\Delta\tilde{S} = \Gamma \Delta C_{\text{P}} \qquad \text{or} \qquad \Gamma = -\frac{\Delta\tilde{S}}{\Delta C_{\text{P}}} \tag{10}$$

When Γ is larger than zero, the $T_{\text{g}}/T_{\text{g}}^{\text{o}} > 1$ and subsequently the $-\Delta S^{\text{glass}} < 0$. Hence, the positive slope, $\Gamma > 0$ reflects the freezing in of degrees of freedom of the polymer chains, and vice versa. Characteristic quantities for both ENR-salt systems at different annealing times are summarized in Table 6. The error of the slope, Γ was estimated by the 2-tailed student *t*-test with 95% confidence level.

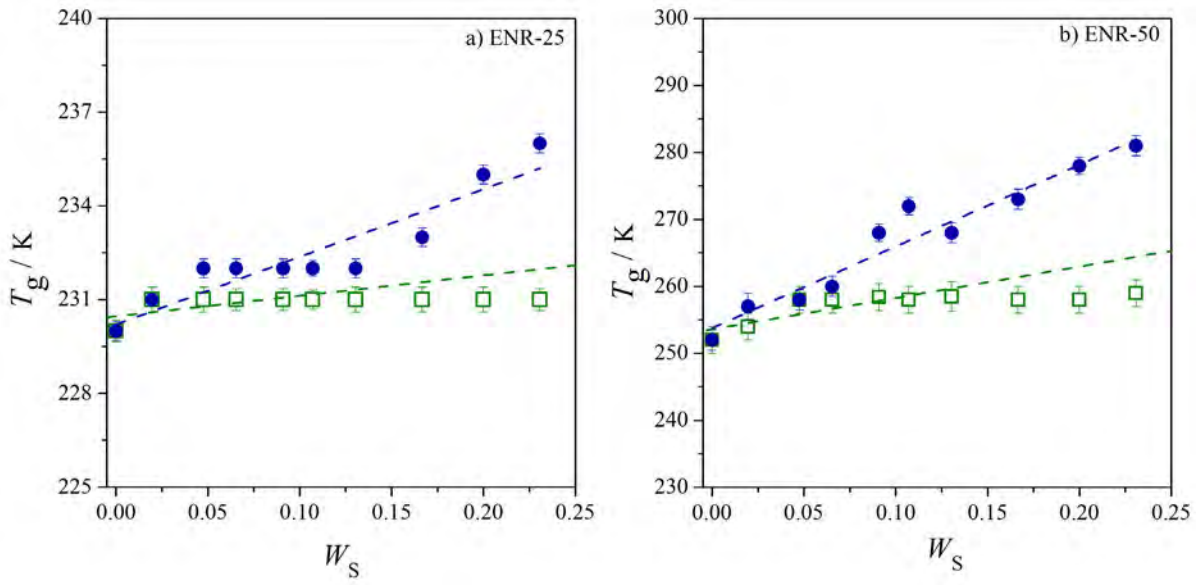

Fig. 6: T_{g} and ΔC_{P} values of (a) ENR-25 and (b) ENR-50 as a function of W_{S} for ENR-salt mixtures annealed at 80°C with different annealing times under N_2 atmosphere, (□) t = 0 hr and, (•) t = 24 h. Dashed lines are the linear regressions after Eq. (9).

Table 6: Characteristics of quantities of the ENR-salt systems.

Polymer	T_{g}^{o} (K)	Γ	$\overline{\Delta C_{\text{P}}}$ (J mol^{-1} K^{-1})	ΔG (kJ mol^{-1})	Correlation coefficient (r^2)
ENR-25, t = 0 h	230	0.03 ± 0.02	68.4 ± 4.0	0.4	0.65
ENR-25, t = 24 h	230	0.08 ± 0.01	62.7 ± 18.7	1.2	0.85
ENR-50, t = 0 h	252	0.18 ± 0.05	61.8 ± 15.5	2.9	0.66
ENR-50, t = 24 h	253	0.39 ± 0.04	78.3 ± 7.4	7.7	0.93

Without thermal treatment, the ENR-25 salt system shows $T_{\text{g}}/T_{\text{g}}^{\text{o}} \approx 1$ which approximately yields $-\Delta S^{\text{glass}} \approx 0$. It reflects the salt behaves neutrally to the polymer. On the other hand, with thermal treatment, the system shows $T_{\text{g}}/T_{\text{g}}^{\text{o}} > 1$ announcing $-\Delta S^{\text{glass}} < 0$ which reflects the freezing in of chain's degrees of freedom. A slightly different behavior is

displayed by the ENR-50-salt systems. The system shows $T_g/T_g^o > 1$ even without thermal treatment, which reflects that salt is slightly active in ENR-50. The freezing in of ENR-50 chain's degree of freedom is further increased with thermal treatment.

The parameter Γ is always higher for ENR-50 as compared to ENR-25. This is due to higher the epoxide content in ENR-50 which may form more intermolecular interactions of salt with the ENR chains. A higher value of Γ is presented for both thermally treated ENR-salt systems as compared to the untreated ENR-salt systems. It implies higher freezing in of chain's degrees of freedom after thermal treatment.

The glass transition is not accompanied by a change in enthalpy. Accordingly, we formulate the related chemical potential or molar partial Gibbs free energy by

$$-\Delta G = -T_g^o \Delta \tilde{S} \tag{11}$$

Eq. (11) reflects the deviation of the state function of the ENR from equilibrium after addition of salt. Following Eq. (11), one observes ENR-salt systems are driven away from equilibrium with salt because the chemical potential is positive. It yields higher value for ENR-50 as compared to ENR-25 due to higher epoxide content. With thermal treatment, the chemical potential becomes higher for both ENR-salt systems which reflects the ENRs are further driven away from equilibrium.

Impedance Spectrocopy

Electrochemical impedance spectroscopy (EIS) was adopted to study the dielectric relaxation of ENR-salt systems. Fig. 7 illustrates the Nyquist plots of *Z′ versus Z″* for both ENR-salt systems at selected salt contents.

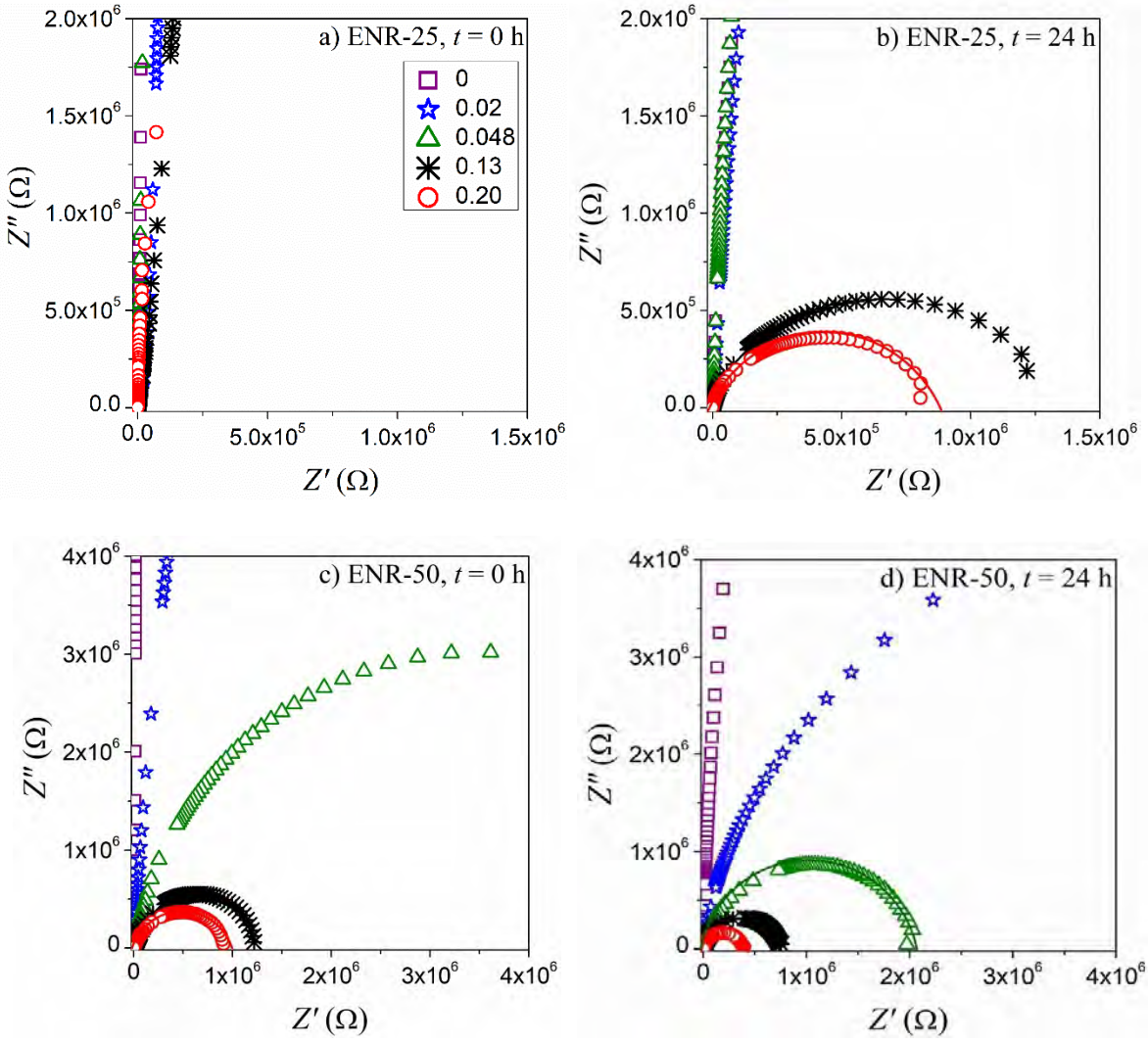

Fig. 7: Nyquist plots of ENR-25 and ENR-50 at selected W_S of different annealing times. The solid curves are the semicircles of the Z'' with their centres and radius at $\frac{R_b}{2}$, where $\left|Z'' - \frac{R_b}{2}\right| = \left(\frac{R_b}{2}\right)^2$.

Both ENR-25 and ENR-50 show inclined spikes starting from origin, which depict that a percolation network has yet to establish in neat ENRs, thus very low ionic conductivities are recorded ($\sigma_{DC} \sim 10^{-11}$ S cm^{-1}, *c.f* Table 7). In general, addition of $LiClO_4$ in ENR promotes the formation of a percolation network at higher salt content, thus leads to the observation of semicircles in Nyquist plots. At W_S = 0.13, ENR-50 exhibits a lower R_b value ($R_b = 5.0\times10^6\ \Omega$) as compared to ENR-25 ($R_b = 4.0\times10^8\ \Omega$) suggesting that ENR-50 shows a slightly higher ionic conductivity (*c.f* Table 6). This may be due to the higher content for epoxide groups, which may serve as the coordination site with salt (which leads to higher T_g) in ENR-50 as compared to ENR-25. Thermal treatment may disrupt the microgel network in ENR-salt systems, thus the solubility of salt in ENR enhances, and consequently an increase in conductivity is observed. Therefore, at W_S = *const*, R_b value of ENR-salt systems with thermal treatment is lower than ENR-salt systems without thermal treatment.

Table 7: Dielectric properties of ENR-salt systems.

ENR-25; t = 0 h							
W_S	f^{Z}_{max}(s^{-1})	Z' (f^{Z}_{max}) (Ω)	R_b (Ω)	σ_{DC} (S cm^{-1})	$f^{Z'\text{-}Z}_{cross}$(s^{-1})	τ^{Z}_{max} (s)	$\tau^{Z'\text{-}Z}_{cross}$ (s)
0	n.a.	n.a.	6.2×10^8	2.2×10^{-11}	n.a.	n.a.	n.a.
0.02	n.a.	n.a.	4.2×10^8	3.0×10^{-11}	n.a.	n.a.	n.a.
0.048	n.a.	n.a.	3.8×10^8	2.3×10^{-11}	n.a.	n.a.	n.a.
0.13	n.a.	n.a.	4.0×10^8	3.0×10^{-11}	n.a.	n.a.	n.a.
0.20	n.a.	n.a.	4.4×10^8	3.0×10^{-11}	n.a.	n.a.	n.a.
ENR-50; t = 0 h							
W_S	f^{Z}_{max}(s^{-1})	Z' (f^{Z}_{max}) (Ω)	R_b (Ω)	σ_{DC} (S cm^{-1})	$f^{Z'\text{-}Z}_{cross}$ (s^{-1})	τ^{Z}_{max} (s)	$\tau^{Z'\text{-}Z}_{cross}$ (s)
0	n.a.	n.a.	5.2×10^8	2.0×10^{-11}	n.a.	n.a.	n.a.
0.02	n.a.	n.a.	2.8×10^8	4.2×10^{-11}	n.a.	n.a.	n.a.
0.048	3.9×10^2	1.2×10^7	2.4×10^7	5.2×10^{-10}	4.5×10^2	4.1×10^{-4}	3.5×10^{-4}
0.13	9.5×10^2	2.5×10^6	5.0×10^6	3.4×10^{-9}	1.2×10^3	1.7×10^{-4}	1.3×10^{-4}
0.20	9.7×10^2	1.7×10^6	3.5×10^6	4.4×10^{-9}	1.6×10^3	1.6×10^{-4}	1.0×10^{-4}
ENR-25; t = 24 h							
W_S	f^{Z}_{max}(s^{-1})	Z' (f^{Z}_{max}) (Ω)	R_b (Ω)	σ_{DC} (S cm^{-1})	$f^{Z'\text{-}Z}_{cross}$ (s^{-1})	τ^{Z}_{max} (s)	$\tau^{Z'\text{-}Z}_{cross}$ (s)
0	n.a.	n.a.	1.0×10^8	1.3×10^{-10}	n.a.	n.a.	n.a.
0.02	n.a.	n.a.	1.0×10^8	1.2×10^{-10}	n.a.	n.a.	n.a.
0.048	n.a.	n.a.	1.0×10^8	8.3×10^{-11}	n.a.	n.a.	n.a.
0.13	4.4×10^2	2.2×10^6	4.5×10^6	3.8×10^{-9}	5.7×10^2	3.6×10^{-4}	2.8×10^{-4}
0.20	6.7×10^2	1.4×10^6	2.8×10^6	5.5×10^{-9}	8.7×10^2	2.4×10^{-4}	1.8×10^{-4}
ENR-50; t = 24 h							
W_S	f^{Z}_{max}(s^{-1})	Z' (f^{Z}_{max}) (Ω)	R_b (Ω)	σ_{DC} (S cm^{-1})	$f^{Z'\text{-}Z}_{cross}$ (s^{-1})	τ^{Z}_{max} (s)	$\tau^{Z'\text{-}Z}_{cross}$ (s)
0	n.a.	n.a.	1.0×10^8	1.0×10^{-10}	n.a.	n.a.	n.a.
0.02	n.a.	n.a.	2.1×10^7	5.7×10^{-10}	8.0×10^1	n.a.	2.0×10^{-3}
0.048	1.3×10^3	3.3×10^6	6.7×10^6	1.9×10^{-9}	1.7×10^3	1.2×10^{-4}	9.3×10^{-5}
0.13	4.3×10^3	6.9×10^5	1.4×10^6	1.1×10^{-8}	5.4×10^3	3.7×10^{-5}	2.9×10^{-5}
0.20	1.2×10^4	4.0×10^5	8.1×10^5	2.1×10^{-8}	1.7×10^4	1.3×10^{-5}	9.6×10^{-6}

n.a. = not detected under the experimental condition

A Bode plot shows frequency information explicity whereas frequency information is hidden in a Nyquist plot. For Bode plots of Z' and Z'' *versus* frequency as shown in Fig. 8, Z' represents the Ohmic resistance of the systems, meanwhile Z'' denotes as the non-Ohmic resistance (*i.e.* capacity resistance as the consequence of samples acting as capacitor). The quantity Z'' displays characteristic frequencies especially for dielectric (or dipole) relaxations resulting from local motion of charged entities. In general, if there is an intersection between Z' and Z'', this suggests the

percolation of charge entities develops [86]. Percolation of charge entities does not develop up to W_S = 0.20 for ENR-25 without thermal treatment as an intersection between Z' and Z'' is not observed [*c.f.* Fig. 8(a)]. This is consistent with the results of a constant T_g = –42 °C for ENR-25-salt systems without thermal treatment for different salt contents [*c.f.* Fig. 6(a)]. A development of a percolation path can be detected at $W_S \geq 0.048$ for ENR-50-salt systems without thermal treatment which is correlated to a sudden increase in T_g at W_S = 0.048 in Fig. 6(b). Thermal treatment disrupts the lightly crosslinked polymer chains, which may enhance the solubility of salt in polymer. Thus, the percolation path develops at lower W_S for both ENR-25-salt systems ($W_S \geq 0.13$) and ENR-50-salt systems ($W_S \geq 0.02$). For systems with no intersection of Z' and Z'', $Z'' > Z'$ within the frequency range studied. Hence, these systems are electric capacitors. Besides, at higher salt content, the difference of Z' and Z'' at $f = const$ at low frequency regime ($f < 10^5$ Hz) (*c.f.* Fig. 8) becomes smaller, which is due to the increase in Z' for both ENR-salt systems.

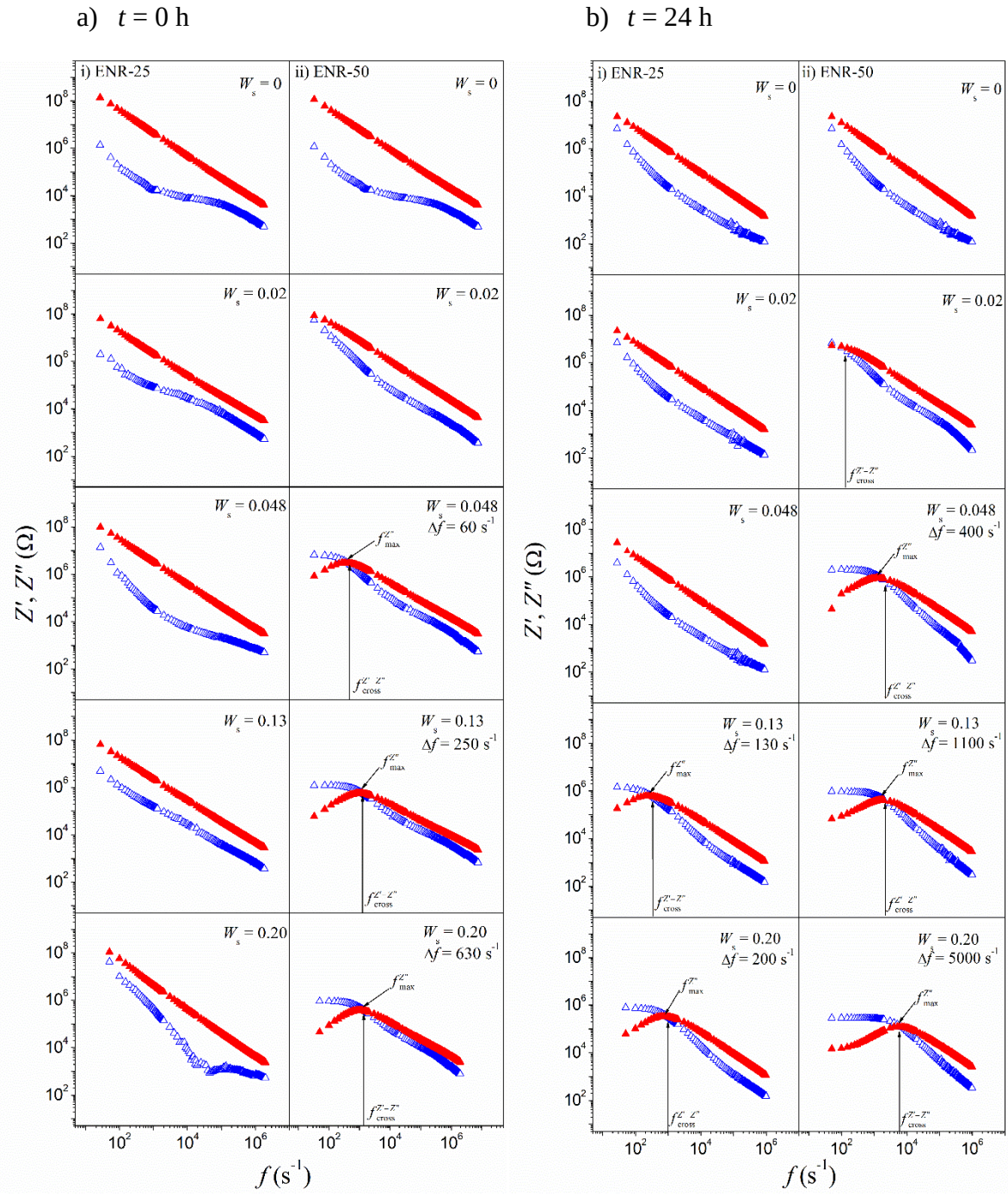

Fig. 8: Bode plots of Z', Z'' *versus* frequency at selected W_S of different annealing times. Solid marker – Z'', open marker

– Z'.

For systems with a development of percolation paths, $f_{\max}^{Z''}$ can be observed under the experimental condition. When $f_{\text{cross}}^{Z'\text{-}Z''} = f_{\max}^{Z''}$, a Debye relaxation of charge entities (*i.e.* just one relaxation time for ideal case) is suggested [74–76]. However, for ENR-salt systems with high salt concentration, $f_{\text{cross}}^{Z'\text{-}Z''} > f_{\max}^{Z''}$ is shown and the distance between $f_{\max}^{Z''}$ and $f_{\text{cross}}^{Z'\text{-}Z''}$ (Δf) is larger at higher salt content (*c.f.* Fig. 8). This implies that the deviation from Debye relaxation increases at higher salt content and thus a broader distribution of relaxation times is noted. We always have dispersion of relaxation times due to the macroscopic dipole (*e.g.* interaction between dipolar entities) in this case. At W_S = *const*, ENR-50 also deviates from a Debye relaxation and shows a distribution of relaxation times where Δf of ENR-50 is larger than ENR-25 due to the association of salt with higher epoxide content in ENR-50.

Besides, $f_{\min}^{Z''}$ is not observed for Z'' as a function of f under the experimental conditions. Negligible electrode polarization is suggested here, because there is no accumulation of dipoles in the interfacial region of the electrode-electrolyte under the experimental condition. This points towards the mobility of the macroscopic dipoles are restricted to localized motions.

Table 7 lists the relaxation times (τ) of the systems. Quantity τ denotes the average time required for the dipole moments of the charge entities to revert to a random distribution after removal of the applied electrical field. ENR-50-salt systems show smaller τ due to higher σ_{DC} (or lower R_b) as compared to ENR-25-salt systems. At higher salt content, τ is smaller at W_S = *const*. Besides, smaller τ is recorded for systems after thermal treatment at W_S = *const*, hence higher conductivity is observed. This observation is may be due to the disruption of the lightly-crosslinked microgel in the thermally treated ENR-salt systems especially for ENR-50 and is correlated to the higher T_g and higher extend of intermolecular interaction (*c.f.* Glass Transition Temperature and Intermolecular Interactions sections) between ENR and charged entities.

Intermolecular Interactions

The intermolecular interactions between salt and ENRs with and without thermal treatment was studied by FTIR spectroscopy. Fig. 9 and Fig. 10 illustrate the FTIR spectra for ENR-25 and ENR-50 at selected salt concentration, respectively. The important absorption bands that will be highlighted are 1664 cm^{-1} and 1069 cm^{-1} which are associated to C=C and C–O–C vibration modes, respectively.

For ENR-25-salt systems without thermal treatment, the absorption band at 1664 cm^{-1} assigned to C=C vibration mode does not show any shift or change in intensity with the addition of salt. However, for $W_S > 0.02$, a new absorption band at 1626 cm^{-1} is observed and increases slightly in absorbance with ascending salt concentration. As for thermally treated ENR-25-salt systems, the 1664 cm^{-1} absorption band is slightly broadened and absorbance of the new absorption band at 1626 cm^{-1} continues to increase progressively with higher salt concentration. It is noteworthy that C=C bonds experience different electron environment in the neighborhood of the epoxide groups. The coordination between salts and epoxide groups causes the vibration mode C=C bonds to shift to lower wavenumbers according to their positions relative to the epoxide group [45]. The absorption band at 1626 cm^{-1} is assigned to the one next to the epoxide group while the broad 1664 cm^{-1} is assigned to the C=C bonds that are further away from the epoxide groups [45]. Thermally treated ENR-25-salt systems show higher absorbance of 1626 cm^{-1} absorption band as compared to the ENR-25-salt systems without thermal treatment which implies more intermolecular interaction of salts with C=C is observed after thermal treatment.

A similar behavior is observed for the ENR-50-salt systems without thermal treatment. The absorption band at 1664 cm^{-1} becomes broadened and a new band at 1620 cm^{-1} increases in absorbance with ascending salt concentration. Interestingly, upon thermal treatment, the absorption band of 1664 cm^{-1} disappears completely and intensity of 1620 cm^{-1} absorption band increases notably. The isothermal treatment at 80 °C may have disrupted the ‘lightly crosslinked´ ENR-50 chains in which may aid more molecular interaction of salt with oxygen atom of epoxide group. Consequently, the absorbance of the absorption band of 1620 cm^{-1} (C=C bond next to epoxide group) increases in thermally treated ENR-50-salt systems. However, no change in the absorbance and band shift for this C=C vibration mode is observed which suggests that salts prefer to coordinate with epoxide oxygen rather than with the C=C bonds.

The absorbance of the band at 1069 cm^{-1} which is assigned to the C–O–C vibration (νC–O–C) of the epoxide group increases with ascending salt concentration for both ENR-25 and ENR-50 without thermal treatment, with more pronounced increment observed in ENR-50. Upon thermal treatment, ENR-25 with salts show an upshifting of the C–O–C absorption band from 1069 cm^{-1} to 1093 cm^{-1}. Meanwhile, ENR-50 shows a downshifting from 1069 cm^{-1} to

1052 cm^{-1}. This downshifting implies that more salts form complexes with epoxide group in thermally treated ENR-50 as compared to thermally treated ENR-25 [45]. This concurs closely with the observations in the variation of T_g and σ_{DC} discussed in section Glass Transition Temperature and Impedance Spectroscopy, respectively.

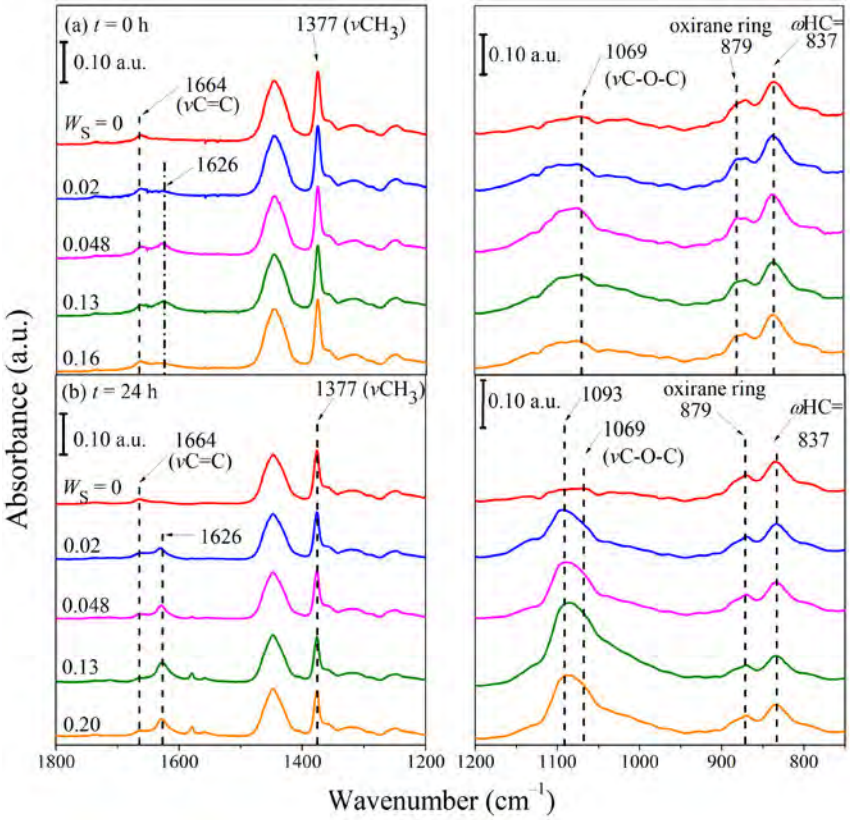

Fig. 9: FTIR spectra of ENR-25-salt systems for (a) t = 0 h and (b) t = 24 h at selected salt concentration.

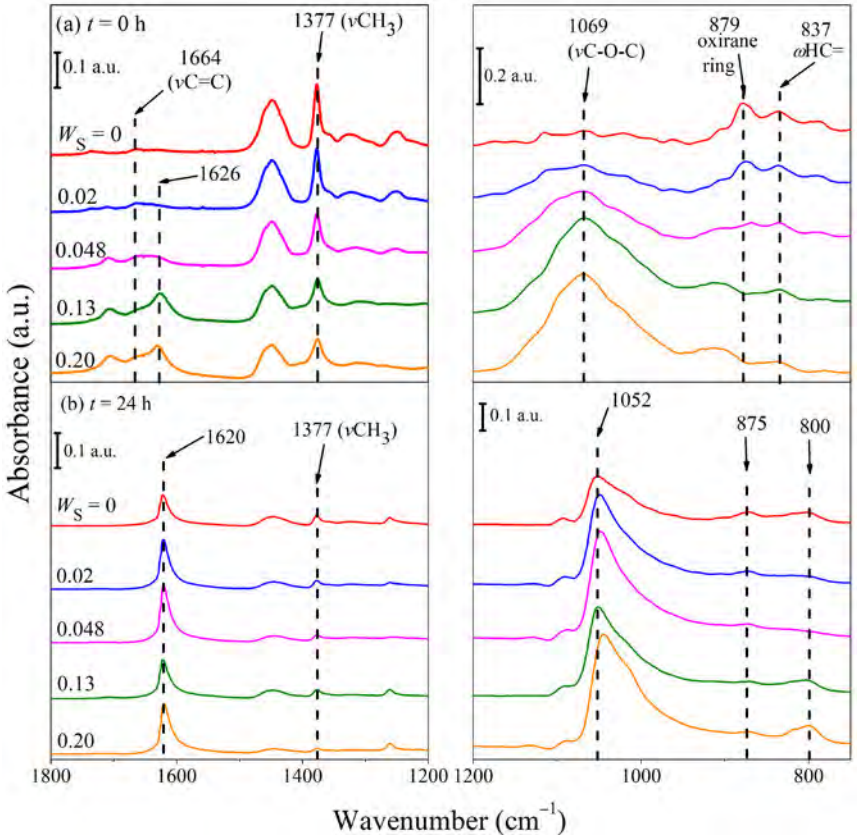

Fig. 10: FTIR spectra of ENR-50-salt systems (a) t = 0 h and (b) t = 24 h at selected salt concentration.

Conclusions

ENR-25 and ENR-50-salt systems were thermally treated at 80 °C for 24 h under inert atmosphere. The 'lightly crosslinked' ENR chains which were formed either through chemical or physical crosslink network of the chains may be disrupted upon thermal treatment and the dissolution of Li salt in ENR may be enhanced. This network disruption is also reflected by the lower thermal stability recorded for both thermally treated ENR-25 and ENR-50. Upon addition of salt into thermally treated ENRs, the increment of T_g with ascending salt concentration is more prominent especially in thermally treated ENR-50. It reflects higher molecular interactions of polymer chains and salt after thermal treatment. Consequently, higher ionic conductivity is exhibited in thermally treated ENRs and more pronounced in thermally treated ENR-50-salt systems. This concurs closely with the FTIR analyses where thermally treated ENRs show spectral changes which imply more molecular interaction of salt and polymer chains. It is deduced that thermal treatment plays an important role in the disruption of 'lightly crosslinked' ENR chains and thus improves the solubility of salt in ENR-salt systems, especially systems with higher epoxide content.

Acknowledgements: The authors would like to thanks Ms. Nurul Syahidah Hussin for the FTIR, TGA, DSC and IS experimental data and the Ministry of Education Malaysia for financing the project under Research Acculturation Grant Scheme (RAGS) (600-RMI/RAGS 5/3 (145/2014)) grant.

References

[1] M. Ravanbakhsh, S. N. Khorasani, S. Khalili, *J. Elastomers Plast.* **48**, 394 (2016).
[2] I. R. Gelling, M. Porter, *Chemical modification of natural rubber*, in: A. Roberts (Ed.), *Nat. Rubber Sci. Technol.*, Oxford University Press, 359, (1990).

[3] R. M. Jorge, L. Lopes, M. R. Benzi, M. T. Ferreira, A. S. Gomes, R. C. R. Nunes, *Int. J. Polym. Mater. Polym. Biomater.* **59**, 330 (2010).
[4] T. Saito, W. Klinklai, S. Kawahara, *Polymer*, **48**, 750 (2007).
[5] I. M. Alwaan, A. Hassan, M. A. M. Piah, *Iran. Polym. J.* **24**, 279 (2015).
[6] K. Ab-Malek, H. R. Ahmadi, A. H. Muhr, I. J. Stephens, J. Gough, J. K. Picken, L. J. Jun, M. U. Zulkefli, I. M. Taib, Seismic Protection of 2nd Penang Crossing Using High Damping Natural Rubber Isolators, *15th World Conf. Earthq. Eng.* 1 (2012).
[7] H. A. M. Hanif, K. C. Yong, *MRB Rubber Technol. Dev.* **18**, 49 (2018).
[8] R. C. Ali, A. Mustafa, F. R. M. Rasdi, *MRB Rubber Technol. Dev.* **18**, 30 (2018).
[9] I. R. Gelling, *Rubber Chem. Technol.* **58**, 86 (1985).
[10] I. R. Gelling, *J. Nat. Rub. Res.* **6**, 184 (1991).
[11] C. S. L. Baker, I. R. Gelling, R. Newell, *Rubber Chem. Technol.* **58**, 67 (1985).
[12] A. S. Hashim, S. K. Ong, Natural Rubber and its Derivatives, In *Elastomers* (N. Cankaya ed.), pp. 159–187 (2017).
[13] T. Johnson, S. Thomas, *Polymer*, **40**, 3223 (1999).
[14] R. Sengupta, S. Chakraborty, S. Bandyopadhyay, S. Dasgupta, R. Mukhopadhyay, K. Auddy, A. S. Deuri, *Polym. Eng. Sci.* **47**, 21 (2007).
[15] T. Johnson, S. Thomas, *Polymer*, **41**, 7511 (2000).
[16] J. E. Davey, M. J. R. Loadman, *Br. Polym. J.* **16**, 134 (1984).
[17] K. Sae-heng, T. Kanya, N. Choothong, K. Kosugi, W. Ariyawiriyanan, S. Kawahara, *Polym. Adv. Technol.* **28**, 1156 (2017).
[18] J. Tangpakdee, Y. Tanaka, *Rubber Chem. Technol.* **70**, 707 (1997).
[19] H. Yu, Z. Zeng, G. Lu, Q. Wang, *Eur. Polym. J.* **44**, 453 (2008).
[20] P. W. Allen, G. M. Bristow, *Rubber Chem. Technol.* **36**, 1024 (1963).
[21] A. H. Eng, Y. Tanaka, S. N. Gan, *J. Nat. Rubber Resour.* **12**, 82 (1997).
[22] E. E. Ehabe, F. Bonfils, J. Sainte-Beuve, A. Collet, F. Schue, *Polym. Eng. Sci.* **46**, 222 (2006).
[23] S. Rolere, C. Bottier, L. Vaysse, F. Bonfils, *Express Polym. Lett.* **10**, 408 (2016).
[24] D. Mekkriengkrai, J. T. Sakdapipanich, Y. Tanaka, *Rubber Chem. Technol.* **79**, 366 (2006).
[25] Y. Tanaka, L. Tarachiwin, *Rubber Chem. Technol.* **82**, 283 (2009).
[26] S. Amnuaypornsri, J. Sakdapipanich, S. Toki, B. S. Hsiao, N. Ichikawa, Y. Tanaka, *Rubber Chem. Technol.* **81**, 753 (2008).
[27] S. Rolere, C. Cazevieille, J. Sainte-Beuve, F. Bonfils, *Eur. Polym. J.* **80**, 117 (2016).
[28] A. Nimpaiboon, S. Amnuaypornsri, J. Sakdapipanich, *Polym. Morphol. Princ. Charact. Process.* **32**, 1135 (2013).
[29] E. Ehabe, Y. Le Roux, F. Ngolemasango, F. Bonfils, G. Nkeng, B. Nkouonkam, M. S. Gobina, *J. Appl. Polym. Sci.* **86**, 703 (2002).
[30] M. Salomez, M. Subileau, J. Intapun, F. Bonfils, L. Vaysse, E. Dubreucq, *J. Appl. Microbiol.* **117**, 921 (2014).
[31] J. Intapun, F. Bonfils, V. Tanrattanakul, E. Dubreucq, L. Vaysse, *J. Appl. Polym. Sci.* **118**, 1341 (2010).
[32] D. S. Campbell, P. S. Farley, *J. Nat. Rubber Res.* **10**, 242 (1995).
[33] W. S. Bahary, L. Bsharah, *J. Polym. Sci. Part A-1*. **6**, 2819 (1968).
[34] S. Rolere, F. Deme, J. Sainte-Beuve, F. Bonfils, *Rubber Chem. Technol.* **90**, 445 (2017).
[35] A. Ahmad, M. Y. A. Rahman, M. L. M. Ali, H. Hashim, F. A. Kalam, *Ionics*, **13**, 67 (2007).
[36] M. Aziz, F. Latif, C. L. Chew, N. Katun, *Solid State Phenom.* **111**, 67 (2006).
[37] S. F. Mohammad, R. Idris, N. S. Mohamed, *Adv. Mater. Res.* **129**–**131**, 561 (2010).
[38] C. H. Chan, H. W. Kammer, *J. Appl. Polym. Sci.* **110**, 424 (2008).
[39] R. Idris, M. . Glasse, R. . Latham, R. . Linford, W. . Schlindwein, *J. Power Sources*. **94**, 206 (2001).
[40] W. Klinklai, S. Kawahara, E. Marwanta, T. Mizumo, Y. Isono, H. Ohno, *Solid State Ionics*. **177**, 3251 (2006).
[41] W. L. Tan, M. Abu Bakar, *Ionics*, **22**, 1319 (2016).
[42] F. Harun, C. H. Chan, *Electronic Applications of Polymer Electrolytes of Epoxidized Natural Rubber and Its Composites*. In Flexible and Stretchable Electronic Composites (D. Ponnamma, K. K. Sadasivuni, C. Wan, S. Thomas, and M. Al-Ali AlMa'adeed, eds), pp. 37–59. Springer International Publishing, (2016).
[43] N. S. Hussin, F. Harun, C. H. Chan, *Macromol. Symp.* **376**, 1700049 (2017).
[44] F. Harun, C. H. Chan, L. H. Sim, T. Winie, N. F. A. Zainal, *AIP Conf. Proc*., 020032 (1–5) (2015).
[45] S. N. H. Mohd Yusoff, L. H. Sim, C. H. Chan, A. Hashifudin, H. -W. Kammer, *Polym. Res. J.* **7**, 159 (2013).
[46] C. H. Chan, H.-W. Kammer, *Polym. Eng. Sci.* **55**, 2250 (2015).
[47] C. H. Chan, H. W. Kammer, L. H. Sim, M. K. Harun, *Blends of Epoxidized Natural Rubber and Thermoplastics*, In *Rubber Types, Properties and Use*, (G. A. Popa, ed.), pp. 306–336. Nova Science

Publishing (2013) .
[48] W. L. Tan, M. Abu Bakar, *Int. J. Electrochem. Sci.* **11**, 8612 (2016).
[49] S. Roy, S. Bhattacharjee, B. R. Gupta, *J. Appl. Polym. Sci.* **49**, 375 (1993).
[50] C. Decker, H. Le Xuan, T. N. Thi Viet, *J. Polym. Sci. Part A Polym. Chem.* **33**, 2759 (1995).
[51] M. R. Ambler, *J. Appl. Polym. Sci.* **20**, 2259 (1976).
[52] W. Klinklai, S. Kawahara, T. Mizumo, M. Yoshizawa, J. T. Sakdapipanich, Y. Isono, H. Ohno, *Eur. Polym. J.* **39**, 1707 (2003).
[53] T. J. Singh, S. V. Bhat, *J. Power Sources*. **129**, 280 (2004).
[54] P. Pal, A. Ghosh, *Solid State Ionics*. **319**, 117 (2018).
[55] S. Wang, Development of Solid Polymer Electrolytes of Polyurethane (dissertation). University of Akron, 2007.
[56] K. Xu, *Chem. Rev.* **104**, 4303 (2004).
[57] F. Wu, R. Chen, F. Wu, L. Li, B. Xu, S. Chen, G. Wang, *J. Power Sources*. **184**, 402 (2008).
[58] W.-H. Hou, C.-Y. Chen, C.-C. Wang, Y.-H. Huang, *Electrochim. Acta*. **48**, 679 (2003).
[59] Y. Tominaga, K. Yamazaki, V. Nanthana, *J. Electrochem. Soc.* **162**, A3133 (2015).
[60] N. Hasan, M. Pulst, M. H. Samiullah, J. Kressler, *J. Polym. Sci. Part B Polym. Phys.* **57**, 21 (2019).
[61] R. J. Seyler, *Assignment of the Glass Transition*, **1249**, ASTM International (1994).
[62] M. Saiter, Jean Marc; Negahban, Mehrdad; dos Santos Claro, P.; Delabarre, P; Garda, *J. Mater. Educ.* **30**, 51 (2008).
[63] C. T. Moynihan, A. J. Easteal, M. A. De Bolt, J. Tucker, *J. Am. Ceram. Soc.* **59**, 12 (1976).
[64] S. I. Abdul Halim, C. H. Chan, H.-W. Kammer, *Polym. Test.* **79**, 105994 (2019).
[65] S. C. Ng, L. H. Gan, *Eur. Polym. J.* **17**, 1073 (1981).
[66] F. Bonfils, A. Doumbia, C. Char, J. Sainte Beuve, *J. Appl. Polym. Sci.* **97**, 903 (2005).
[67] N. V. Bac, L. Terlemezyan, M. Mihailov, *J. Appl. Polym. Sci.* **50**, 845 (1993).
[68] N. V. Bac, L. Terlemezyan, M. Mihailov, *J. Appl. Polym. Sci.* **42**, 2965 (1991).
[69] N. T. Ha, N. H. Quan, C. H. Ha, N. P. D. Linh, P. T. Nghia, *Vietnam J. Sci. Technol.* **56**, 169 (2018).
[70] J. H. Bradbury, M. C. S. Perera, *J. Appl. Polym. Sci.* **30**, 3347 (1985).
[71] S. Roy, B. R. Gupta, B. R. Maiti, *J. Elastomers Plast.* **22**, 280 (1990).
[72] J. H. Aklonis, W. J. MacKnight, M. Shen, W. P. Mason, *Phys. Today*. **26**, 249 (1973).
[73] E. Kalkornsurapranee, W. Yung-Aoon, L. Songtipya, J. Johns, *Plast. Rubber Compos.* **46**, 258 (2017).
[74] R. Stephen, S. Jose, K. Joseph, S. Thomas, Z. Oommen, *Polym. Degrad. Stab.* **91**, 1717 (2006).
[75] J. Johns, C. Nakason, A. Thitithammawong, P. Klinpituksa, *Rubber Chem. Technol.* **85**, 565 (2012).
[76] C. Kirsch, M. Pulst, M. H. Samiullah, P. Ruda, N. Hasan, J. Kressler, *Solid State Ionics*. **309**, 163 (2017).
[77] M. Sonderegger, J. Roos, C. Kugler, M. Mali, D. Brinkmann, *Solid State Ionics*. **53**–**56**, 849 (1992).
[78] X. Ao, X. Wang, J. Tan, S. Zhang, C. Su, L. Dong, M. Tang, Z. Wang, B. Tian, H. Wang, *Nano Energy*. **79**, 105475 (2021).
[79] J. Peng, Y. Xiao, D. A. Clarkson, S. G. Greenbaum, T. A. Zawodzinski, X. C. Chen, *ACS Appl. Polym. Mater.* **2**, 1180 (2020).
[80] R. Zhang, Z. Wei, W. Lei, T. Jiang, Q. Zhang, D. Shi, *Chem. ElectroChem.* **7**, 3353 (2020).
[81] E. A. Dimarzio, J. H. Gibbs, *J. Polym. Sci. Part A Gen. Pap.* **1**, 1417 (1963).
[82] S. Lascaud, M. Perrier, A. Vallée, S. Besner, J. Prud'homme, M. Armand, *Macromolecules*. **27**, 7469 (1994).
[83] C. A. Angell, C. Liu, E. Sanchez, *Nature*. **6416**, 137 (1993).
[84] S. Besner, J. Prud'homme, *Macromolecules.* **22**, 3029 (1989).
[85] S. Besner, A. Vallée, G. Bouchard, *Macromolecules*. **25**, 6480 (1992).
[86] C. H. Chan, H. Kammer, *Pure Appl. Chem.* **90**, 939 (2018).
[87] C. H. Chan, H. W. Kammer, L. H. Sim, S. N. H. M. Yusoff, A. Hashifudin, T. Winie, *Ionics.* **20**, 189 (2014).
[88] C. H. Chan, H.-W. Kammer, *Ionics*, **21**, 927 (2015).
[89] P. Debye, Reprinted 1954 in Collected Papers of Peter J. W. Debye. Interscience, New York. *Ver. Deut. Phys. Gesell.* **15**, 777 (1913).